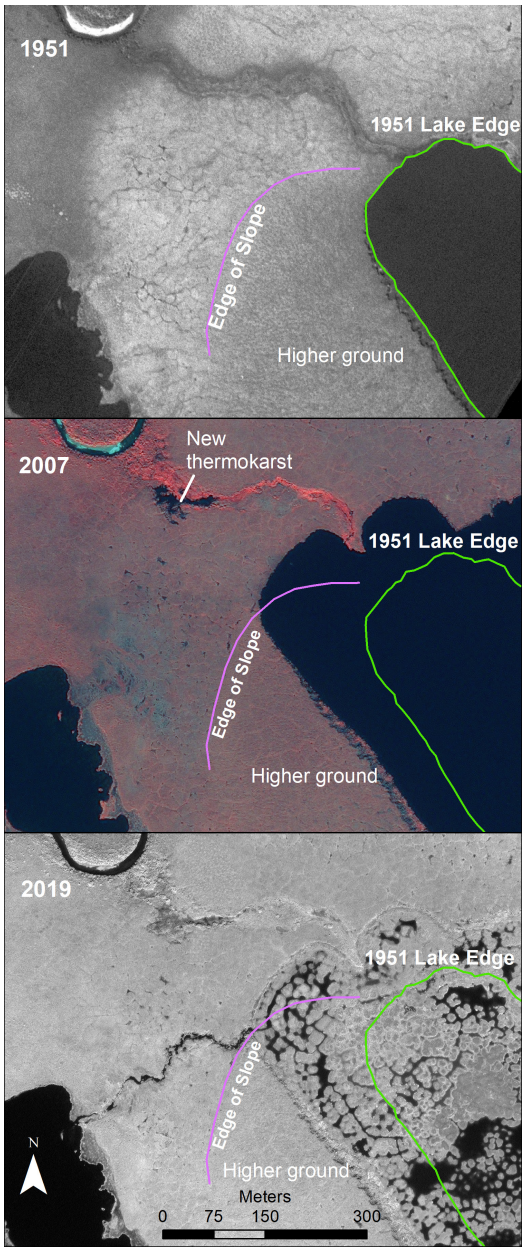
National Park Service
U.S. Department of the Interior

Natural Resource Stewardship and Science

Stability of Ice Wedges in Alaska's Arctic National Parks, 1951-2019

Natural Resource Report NPS/ARCN/NRR—2022/2383



ON THE COVER

Channel formation and lake drainage along degraded ice wedges in the Noatak National Preserve. This area had scattered small thermokarst pits due to ice-wedge degradation on the 1951 aerial photograph (upper) that changed little through the 2007 IKONOS image (center) and 2019 Worldview-2 image (lower). New thermokarst is visible in 2007 in the form of an intricate pond along the original drainage channel leading from the north end of the lake (which is bright red color due to shrubs). This thermokarst surprisingly did not visibly affect the lake level. However, north- and westward advance of the lakeshore edge after 1951 opened up a drainage pathway through degraded ice wedges north and west of the higher ground west of the lake, and this allowed the lake to drain between 2007 and 2019. View is centered near longitude -162.520, latitude 67.550.
Images U.S. Geological Survey (2018) and Satellite Imaging Corporation (2022a, b)

Stability of Ice Wedges in Alaska's Arctic National Parks, 1951-2019

Natural Resource Report NPS/ARCN/NRR—2022/2383

David K. Swanson

[1]National Park Service
4175 Geist Road
Fairbanks, AK 99708

May 2022

U.S. Department of the Interior
National Park Service
Natural Resource Stewardship and Science
Fort Collins, Colorado

The National Park Service, Natural Resource Stewardship and Science office in Fort Collins, Colorado, publishes a range of reports that address natural resource topics. These reports are of interest and applicability to a broad audience in the National Park Service and others in natural resource management, including scientists, conservation and environmental constituencies, and the public.

The Natural Resource Report Series is used to disseminate comprehensive information and analysis about natural resources and related topics concerning lands managed by the National Park Service. The series supports the advancement of science, informed decision-making, and the achievement of the National Park Service mission.

All manuscripts in the series receive the appropriate level of peer review to ensure that the information is scientifically credible and technically accurate.

Views, statements, findings, conclusions, recommendations, and data in this report do not necessarily reflect views and policies of the National Park Service, U.S. Department of the Interior. Mention of trade names or commercial products does not constitute endorsement or recommendation for use by the U.S. Government.

This report is available in digital format from NPS Arctic Inventory and Monitoring program's Terrestrial Landscape Patterns and Dynamics website and the Natural Resource Publications Management website. If you have difficulty accessing information in this publication, particularly if using assistive technology, please email irma@nps.gov.

Please cite this publication as:

Swanson, D. K. 2022. Stability of ice wedges in Alaska's Arctic National Parks, 1951-2019. Natural Resource Report NPS/ARCN/NRR—2022/2383. National Park Service, Fort Collins, Colorado. https://doi.org/10.36967/nrr-2293324.

NPS 953/180404, May 2022

Contents

Page

Figures....iv

Tables....v

Abstract....vi

Acknowledgments....vi

List of Term and Acronyms....vii

Introduction....1

Methods....5

Study Areas....5

Ahnewetut Wetlands, Kobuk Valley National Park....5

Lower Noatak Lowlands, Noatak National Preserve....6

Coastal Plain, Bering Land Bridge National Preserve....8

Climate....10

Analytical Methods....12

Historical Aerial Photograph Preparation....12

IKONOS Image Preparation....13

Worldview-2 Image Preparation....14

Plot Establishment....14

Identification of Ice-Wedge Polygon Zones....16

Mapping of Ice-Wedge Polygon Pits and Ponds....16

Compute and Analyze the Position Index of Water Pixels....16

Visual Assessment of Ice-Wedge Polygons....17

Visual Assessment of ice-wedge drainage channels....17

Results....19

Discussion and Conclusions....26

Literature Cited....27

Figures

Page

Figure 1. Location of the study areas in the National Park Service units of the Arctic Inventory and Monitoring Network. 1

Figure 2. Ice-wedge polygons in the Lower Noatak Lowlands study area in NOAT. 2

Figure 3. An example of a small pond formed by ice-wedge degradation in the KOVA study area (photo date 2 Aug 2012). 3

Figure 4. Overview of the Ahnewetut Wetlands study area in Kobuk Valley National Park. 6

Figure 5. The Lower Noatak Lowlands subsection study area of the Noatak National Preserve (NOAT). 7

Figure 6. The BELA study area. Dots mark remotely sensed plot locations. 9

Figure 7. Mean annual air temperature vs. year in Kotzebue, Alaska. 10

Figure 8. Annual sum of thaw degree-days vs. year in Kotzebue, Alaska 11

Figure 9. Annual total precipitation in Kotzebue, Alaska. 12

Figure 10. Computation of the water pixel position index 17

Figure 11. Summary of ice-wedge polygon types from visual assessment. 20

Figure 12. Water distribution by ice-wedge polygon sector. 21

Figure 13. History of KOVA study area plot 63. Ice-wedge polygon marginal ponds formed between 1952 and 2007, and enlarged further between 2007 and 2020 22

Figure 14. History of NOAT study area plot 26. 23

Figure 15 (following page). Channel formation and lake drainage along degraded ice wedges in NOAT. 24

Tables

Page

Table 1. Dates of imagery used in this study[A] 13

Table 2. Plot Properties 15

Table 3. Summary of ice-wedge polygon water mapping 19

Table 4. Summary of Water Distance Indices by Study Area and Sampling Episode 19

Table 5. Water Distance Indices and Fires in the NOAT study area 23

Table 6. Dimensions of new drainage channels observed between IKONOS 2006-09 and WV-2 2019-2020 images 24

Abstract

Ice-wedge polygons are a striking and widespread feature of the arctic landscape. Ice wedges are vulnerable to thaw because they are nearly pure ice bodies near the surface, with little insulating overlying material. Ice-wedge polygon monitoring is a part of the permafrost monitoring program for the National Park Services Arctic Inventory and Monitoring Network (ARCN, the five National Park units in northern Alaska). The present report is a re-analysis of ice-wedge condition in three study areas, based on satellite images taken in 2019 and 2020 (sampling episode 3). Results are compared to previous analyses based on aerial photographs from 1950-51 (episode 1) and satellite images from 2006-2009 (episode 2). Significant ice-wedge degradation occurred between sampling episodes 1 and 2 in one of the study areas (in Kobuk Valley National Park, KOVA). Sampling episode 3 revealed relatively minor changes from episode 2 in all three areas. This is somewhat surprising given the record warm temperatures that occurred between sampling episodes 2 and 3. Apparently the recent warming did not cross any thresholds that would trigger immediate and widespread visible changes in ice wedges, or insufficient time has elapsed since the recent onset of warmer temperatures in 2014. However, the effects of previous ice-wedge degradation continued to be manifested in new drainage channels that formed by linkage of pits from previous ice-wedge degradation. The Noatak National Preserve (NOAT) study area was affected by wildfires in 1977 and 2010, and comparison of burned to unburned areas in subsequent sampling episodes failed to show significant new ice-wedge degradation brought about by these fires.

Acknowledgments

Thanks to Jon O’Donnell for helpful review comments.

List of Term and Acronyms

Active layer. Ground above permafrost that thaws each summer.

ARCN. The NPS Arctic Inventory and Monitoring Network.

BELA. Bering Land Bridge National Preserve.

Color-infrared. Refers to images that contain data from visible light and the near infrared wavelength bands (invisible to the human eye, with wavelengths longer than those of red color). To enable printing or screen projection of these images by a red-green-blue color scheme, the infrared, red, and green data are portrayed using red, green, and blue colors, respectively.

Epigenetic. Refers to ice wedges that formed after deposition of the enclosing material was complete (van Everdingen 1998). Contrasts with *syngenetic*.

High-center ice-wedge polygon. Ice-wedge polygon with high center sloping out to a lower marginal trough, often but not always produced by degradation of ice wedges.

Ice wedges. Ground ice formed by contraction cracking of frozen ground in the winter followed by infilling with water that freezes and is preserved in permafrost. The surface manifestation of actively growing ice wedges as viewed from above is ice-wedge polygons.

Holocene. The most recent geologic epoch, extending from 11,700 years ago to the present (Cohen et al. 2013). The Holocene was a time of relatively stable warm climate, after the last Pleistocene glacial episode.

IKONOS. A commercial satellite that collected multispectral (multiple wavelengths of light) imagery with 4-m resolution that can be pan-sharpened (enhanced using higher-resolution panchromatic data) to 1-m resolution (Satellite Imaging Corporation 2022a).

KOVA. Kobuk Valley National Park.

Low-center ice wedge polygon. Ice-wedge polygon with central depression and low ridges along the polygon margins.

NOAT. Noatak National Preserve.

NPS. National Park Service

Permafrost. Ground that remains below 0° C for two or more consecutive years (van Everdingen 1998). In ARCN most permafrost has been frozen for thousands of years and is many meters thick.

Pleistocene. The geologic epoch extending from 2.58 million to 11,700 years ago and characterized by multiple cold periods known informally as "ice ages" (Cohen et al. 2013).

Subsection. Short for "ecological subsection", a unit of terrain in the National Hierarchical Framework of Ecological Units (Cleland et al. 1997).

Syngenetic. Refers to ice wedges that formed in material as it was accumulating. Syngenetic ice wedges grow upward as material accumulates and thus reach greater vertical dimensions than epigenetic ice wedges (van Everdingen 1998).

Thaw degree-days. Sum of daily positive temperatures (in degrees C) through the year.

Thermal erosion. Erosion that occurs in frozen materials by the combined action of thaw and mechanical action of moving water.

Thermokarst. Subsidence due to thaw of ice in the ground.

WV-2. Worldview 2A commercial satellite that collects multispectral (multiple wavelengths of light, 1.84 m resolution) and panchromatic (black-and-white, 0.46 m resolution) imagery (Satellite Imaging Corporation 2022b).

Introduction

Ice-wedge polygons are a striking and widespread feature of the arctic landscape. They form when frozen ground cracks due to contraction in the winter, the cracks fill with ice, and the resulting wedge of ice is preserved in permafrost (Leffingwell 1915; Lachenbruch 1963). After many years of cracking in approximately the same place, ice wedges can become a meter or more wide at the top. These ice wedges are vulnerable to thaw because they are nearly pure ice bodies near the surface, with little insulating overlying material. Surface disturbance or a warm weather can cause them to thaw and produce surface subsidence (Kanevskiy et al. 2017). Multiple studies have reported significant degradation of ice wedges on the North Slope of Alaska in recent decades (Jorgenson, Shur, and Pullman 2006; Jorgenson et al. 2015; B. M. Jones et al. 2015; Liljedahl et al. 2016; Kanevskiy et al. 2017). (Necsoiu et al. 2013) reported ice-wedge degradation in a small study area in Kobuk Valley National Park. Because of the sensitivity of ice wedges to thaw, ice-wedge polygon monitoring is a part of the permafrost monitoring program for the National Park Services Arctic Inventory and Monitoring Network (ARCN, the five National Park units in northern Alaska; Fig. 1). The present study was carried out as a part of ARCN permafrost monitoring (Swanson 2017a; Swanson 2017b). It is a re-analysis of ice-wedge condition in three study areas, undertaken using imagery taken approximately 10 years after the imagery used in the next most recent monitoring analysis (Swanson 2016).

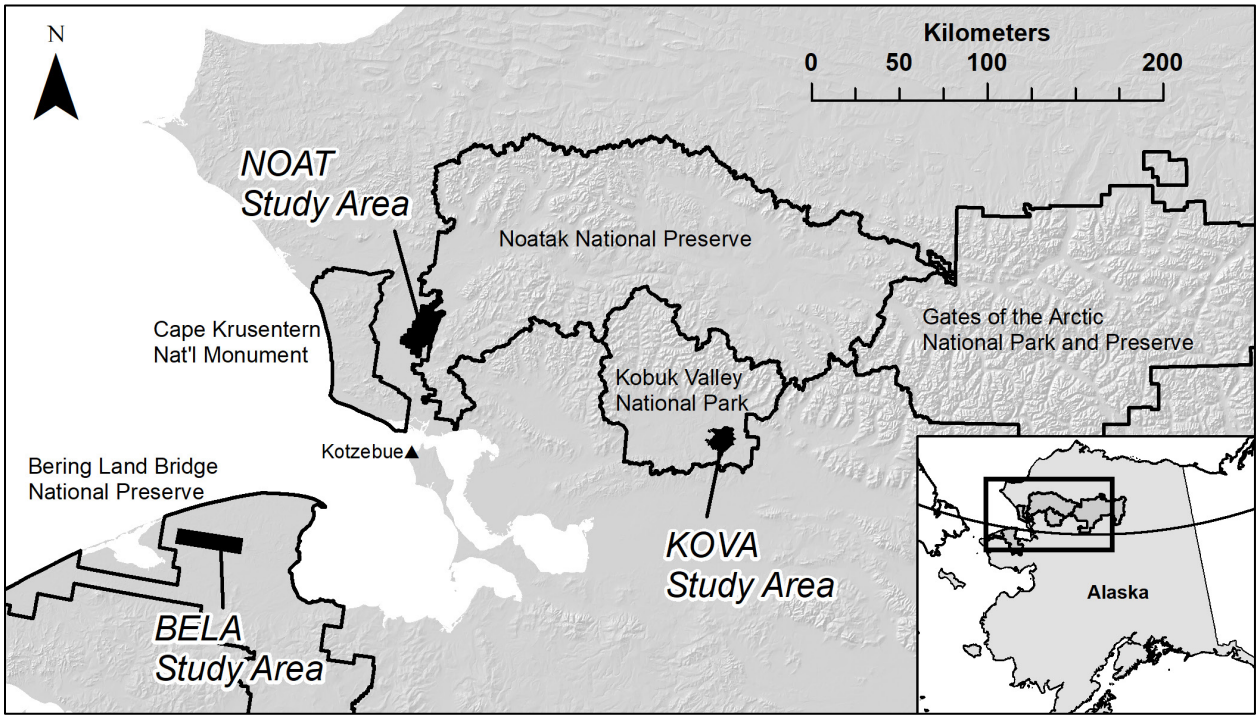


Figure 1. Location of the study areas in the National Park Service units of the Arctic Inventory and Monitoring Network.

Actively growing ice-wedge polygons typically have low ridges, on both sides of the wedge, that are higher than the polygon center; hence the name “low-center ice wedge polygon” (van Everdingen 1998). In poorly drained permafrost lowlands, low-center polygons often have wet soils or standing water in the polygon centers, ringed by the higher margins, and a narrow wet trench centered over the wedge (Fig. 2).

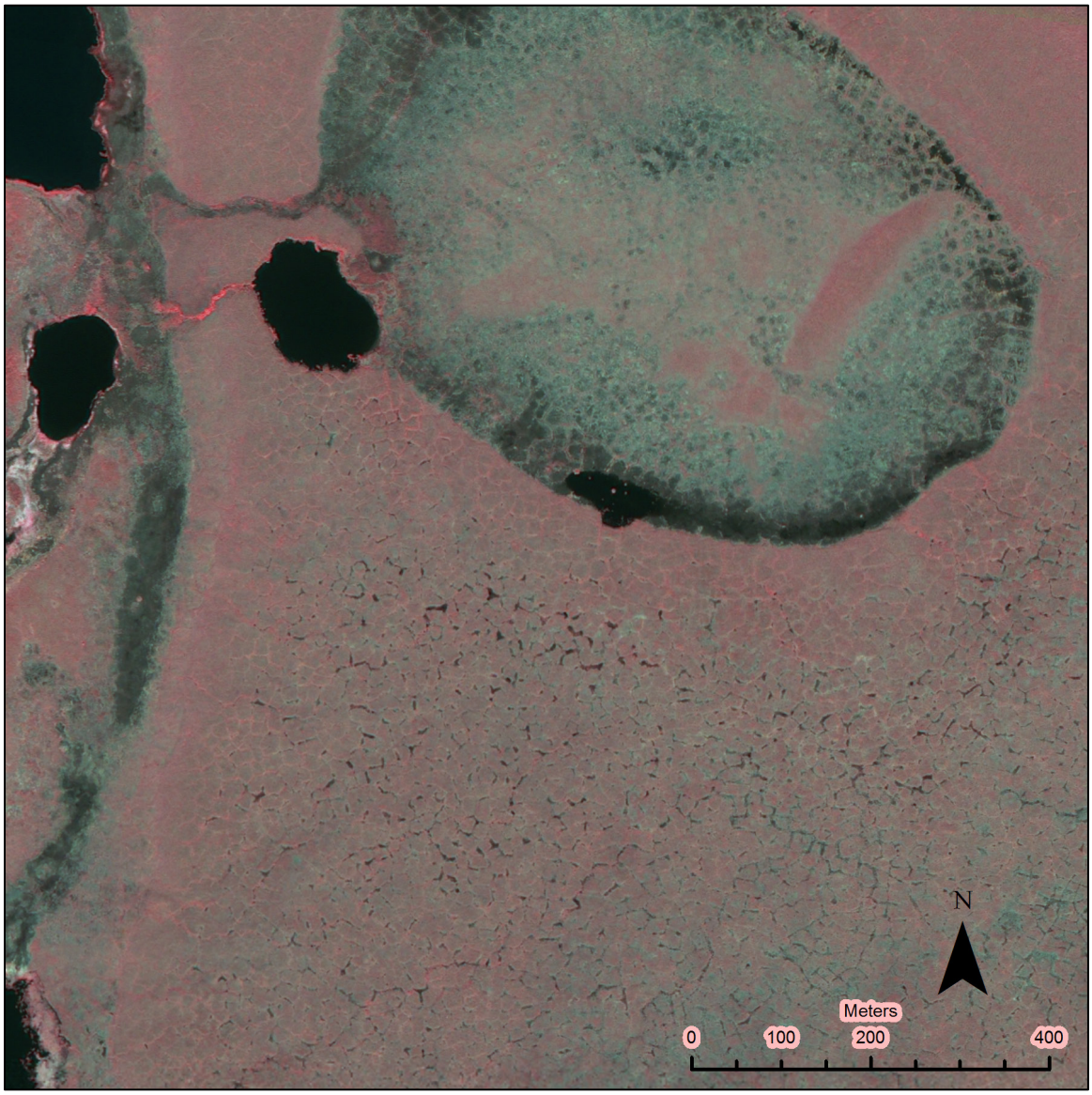


Figure 2. Ice-wedge polygons in the Lower Noatak Lowlands study area in NOAT. A drained lake with low-center polygons is visible in the northern part of this IKONOS image (3 July 2007). High-center ice wedge polygons with numerous ponds due to degradation of ice wedges are visible in the southern half of the image. In this color-infrared color scheme, green vegetation appears red and water is black.

When an ice wedge melts, subsidence occurs over and adjacent to the wedge, i.e. around the polygon margin. A polygon where the wedge has melted due to thaw of permafrost typically has small oblong

ponds over the degraded wedges; larger ponds sometimes form at wedge junctions (Figs. 2, 3). Subsidence due to thaw of ground ice is called thermokarst (Czudek and Demek 1970). Subsidence along the wedges often results in high-center ice-wedge polygons (van Everdingen 1998). High-center polygons are driest in the center and wetter around the margins. Initial ice-wedge degradation results in high-center polygons with disconnected ponds in the marginal troughs; with continued degradation the ponds may become connected and increase surface runoff (Liljedahl et al. 2016).



Figure 3. An example of a small pond formed by ice-wedge degradation in the KOVA study area (photo date 2 Aug 2012). Elongated ponds form over degraded ice wedges, these are about 1 m wide and several meters long. Right-angle intersections such as this one are common.

The presence or absence of ponds formed by ice-wedge degradation can be determined by analysis of high-resolution aerial photographs and satellite images (Jorgenson, Shur, and Pullman 2006; Liljedahl et al. 2016). Wet areas with tundra vegetation are readily visible as darker tones on images. The present report assesses the degradation of ice wedges in three study areas in ARCN by mapping surface water within ice-wedge polygons. The absolute area of water in polygon vicinities varies with time of year and weather, and it is difficult to determine precisely, due to overlap in the appearance of saturated peaty soils, shallow water over vegetation, shallow water with floating or emergent vegetation, and deeper water. Thus our monitoring protocol emphasizes the location of water within polygons (on margins vs. in centers) rather than the absolute area of water cover, to assess ice-wedge polygon degradation.

The purpose of the present report is to present analysis of ice-wedge condition on a new generation of imagery from 2019-2020 (hereafter known as "episode 3") and compare it to the previous ice-wedge assessments based on 1951-52 (episode 1) and 2006-2009 (episode 2) images. This analysis was carried out in three study areas located in in Bering Land Bridge National Preserve (BELA), Kobuk Valley National Park (KOVA), the Noatak National Preserve (NOAT). The BELA study area is new to this report because it did not have 1951-52 images available; the first two episodes at the other two study areas were reported in (Swanson 2016).

Methods

Study Areas

Ahnewetut Wetlands, Kobuk Valley National Park

Ice wedge polygons with visible surface manifestations are not widespread in KOVA. They occur almost exclusively in the Ahnewetut Wetland ecological subsection (Figs. 1 and 4) (Swanson 2001). This subsection covers 142 km^2 and is a region of numerous lakes with wetlands in between, on sandy sediments near the Great Kobuk Sand Dunes. While the lowlands in KOVA are mostly forested, the wetland areas with permafrost and thin active layers where ice-wedge polygons occur are mostly treeless. In the forested environments of Interior Alaska, ice wedges are generally inactive or weakly active (and thus quite inconspicuous), while ice wedges in arctic Alaska are active and conspicuous; the transition occurs near the KOVA study area (Péwé 1975; Jorgenson et al. 2008). The Ahnetwetut Wetlands ice-wedge polygon field is the last dense network of ice-wedge polygons with clear surface manifestation that one observes when flying to the south and east in this part of the Kobuk Valley, suggesting that these wedges are near the recent climatic limit of active ice-wedge growth.

Twelve soil pits dug in ice-wedge polygon terrain near the center of the Ahnewetut Wetlands as a part of another study (Swanson 2013) between 31 July and 2 Aug 2012 were frozen at depths ranging from 36 to 80 cm, and most had water within 30 cm of the surface. Six of these pits had organic soil material (peat) down to the frozen layer, and the other six had sandy sediments under 30-45 cm of peat. Vegetation consisted of cottonsedge (*Eriophorum vaginatum*), various *Carex* sedge species, low shrubs (*Betula nana*, *Vaccinium uliginosum*, *Andromedra polifolia*), and mosses, predominantly *Sphagnum* sp.

The sandy sediments are interpreted as sand sheet deposits and alluvium, and they are adjacent to the Great Kobuk Sand Dunes (Mann, Heiser, and Finney 2002). This study area was not glaciated at the time of the last glacial maximum (Péwé 1975), but the ice wedges there are nonetheless interpreted to be Holocene epigenetic wedges, with minor syngenesis linked to Holocene peat accumulation. Thermokarst features indicative of large syngenetic ice wedges are lacking in the immediate study area. The lakes in the Ahnewetut Wetlands are sandy bottomed with relatively stable, vegetated shorelines. Most of the land between the lakes does not show outlines from the former shores of drained lakes, in contrast to the other two study areas.

The southeast edge of the Ahnewetut Wetlands study area was burned by a lightning-caused wildfire in 1971 (Alaska Interagency Coordination Center 2021). Just 7 of our 300 plots are both within the fire perimeter and cloud-free, and of these only two had visible ice-wedge polygons, so no comprehensive test of this fire's effect on ice-wedge polygons was possible.

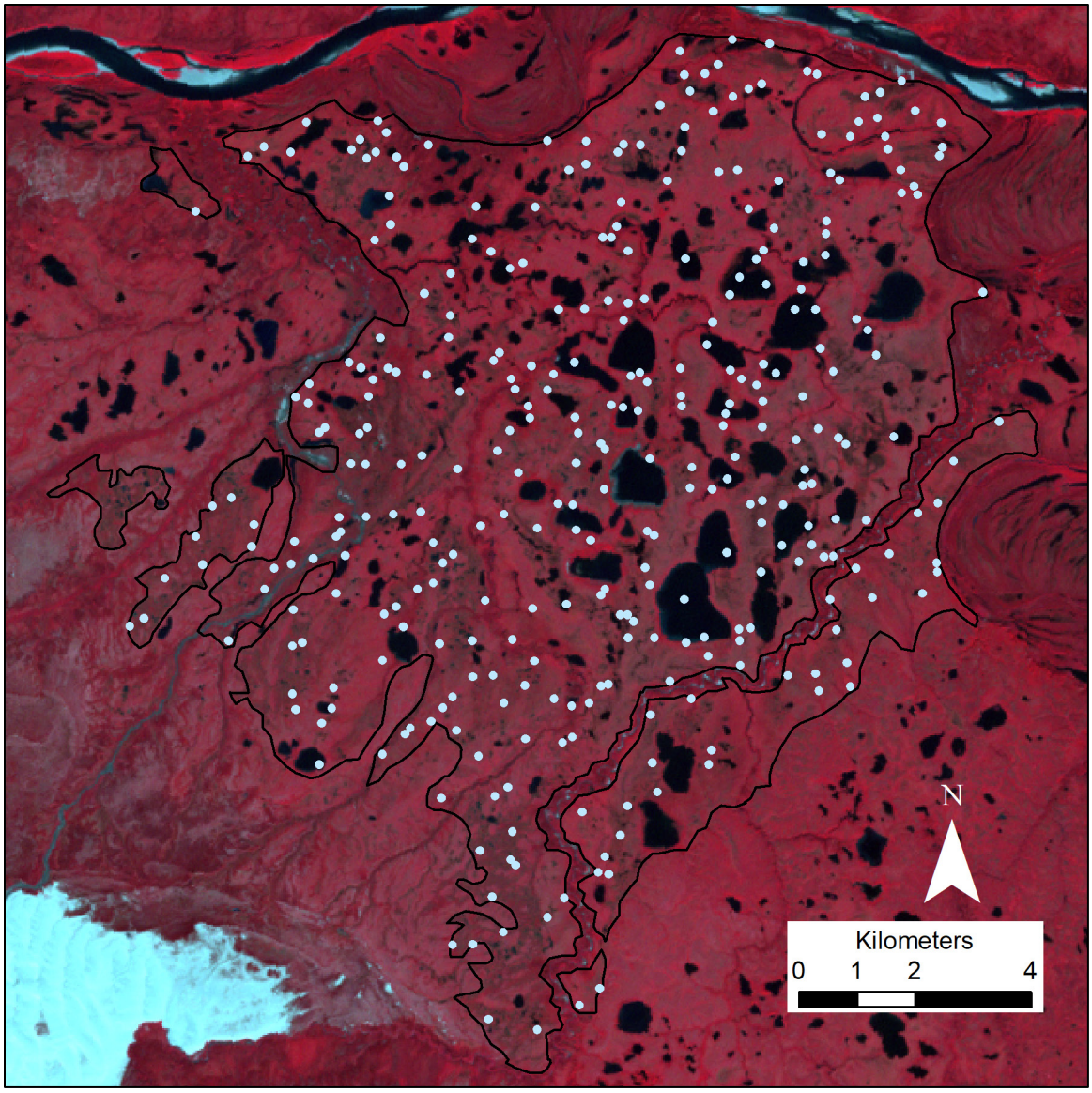


Figure 4. Overview of the Ahnewetut Wetlands study area in Kobuk Valley National Park. The Ahnewetut Wetlands subsection is outlined in black, and dots mark remotely sensed plot locations. Lakes appear black, and the white area southwest of the study area is the Great Kobuk Sand Dunes. The background image here is a Landsat mosaic from the early 2000s, displayed in a color-infrared color scheme.

Lower Noatak Lowlands, Noatak National Preserve

Ice-wedge polygons are common in the lowlands of NOAT, but visible polygons occur mostly in patches of 1 km^2 or less; the exception is the Lower Noatak Lowlands subsection (Figs. 1 and 5) (Jorgenson, Swanson, and Macander 2001). The Lower Noatak Lowlands is a region of numerous thermokarst lakes and overlapping drained lake basins, with visible ice-wedge polygons on most of the land surface except recently drained lake basins (Fig. 5). The portion of the Lower Noatak Lowlands where I sampled (clipped to NPS boundaries and available 1950s images) occupies 267 km^2. The study area is in the southwestern part of NOAT, which has the Preserve's warmest climate, and vegetation is a mix of boreal forest and arctic tundra. This subsection was selected for analysis

because it was the only place in the Preserve where the area and density of ice-wedge polygons made sampling practical.

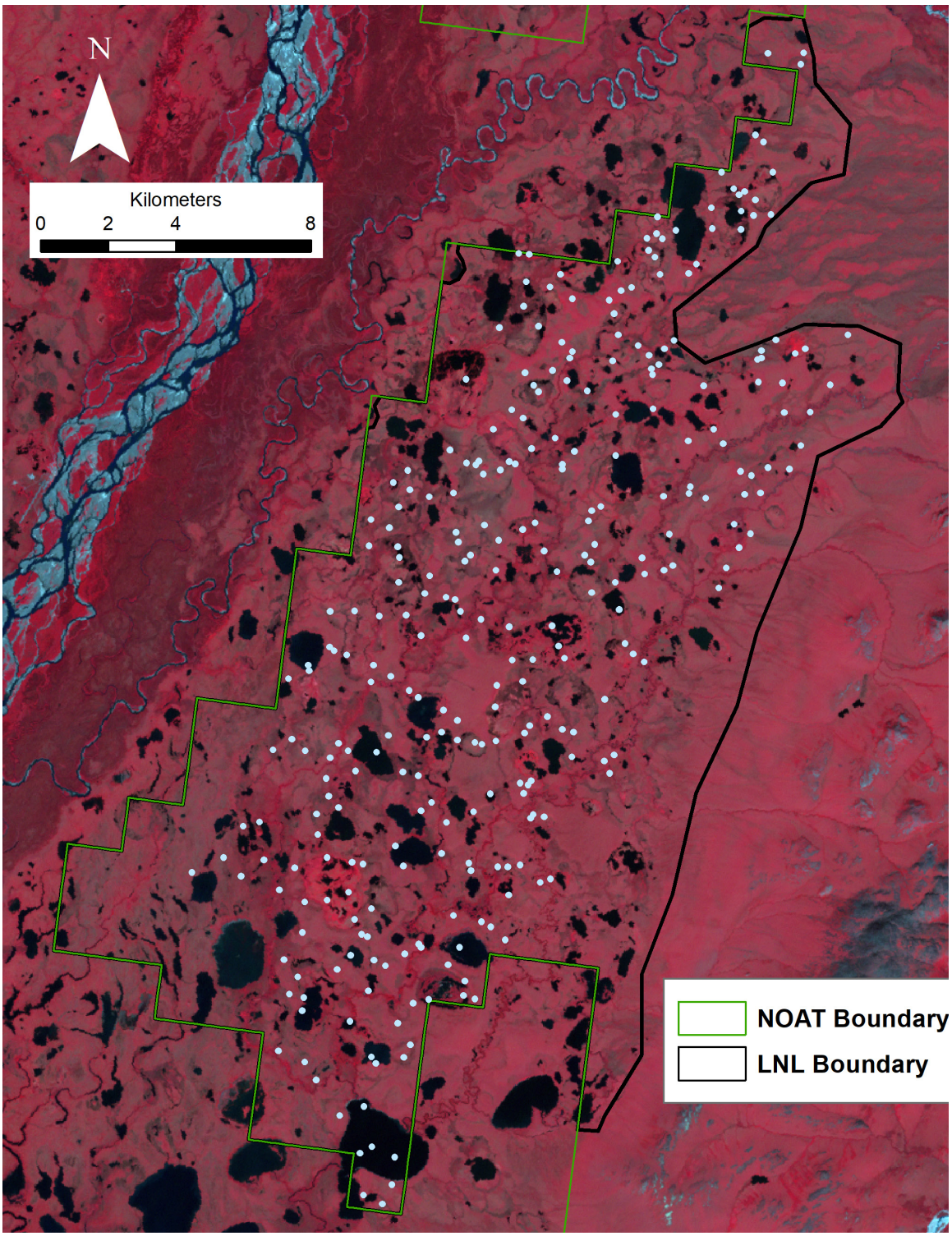


Figure 5. The Lower Noatak Lowlands subsection study area of the Noatak National Preserve (NOAT). The Lower Noatak Lowlands subsection (LNL) is outlined in black, and dots mark remotely sensed plot locations.

Fourteen soil pits that were dug in polygon terrain in the Lower Noatak Lowlands as a part of another study (Swanson 2013) in early August 2013 showed frozen soil within 50 cm of the soil surface and free water perched above the frozen soil in all cases. The surface organic layer was 20 to 45 cm thick in 13 of the pits and over 45 cm thick but unknown (due to frozen soil) in one. The underlying mineral soil consisted of silt loam, probably lacustrine sediment. Vegetation was cottonsedge (*Eriophorum vaginatum*), various *Carex* sedge species, and low shrubs from the family *Ericaceae* (*Vaccinium uliginosum*, *Vaccinium vitis-idaea*, *Andromedra polifolia*), and mosses, predominantly *Sphagnum* sp. White spruce (*Picea glauca*) forest is present on well-drained soils of the Noatak River floodplain to the west of the study area.

The NOAT study area is underlain mostly by lacustrine deposits of uncertain Holocene to Late Pleistocene age (Hamilton 2010). While thermokarst is ubiquitous across this study area, indicating ice-rich ground, the thermokarst depressions have relatively low relief of just a few meters. Outlines of drained lakes cover most of the study area, indicating reworking of the surface by thermokarst in the Holocene. Thus here, as in the Ahnewetut Wetlands study area, the ice wedges are interpreted to be Holocene epigenetic wedges, with minor syngenesis linked to Holocene peat accumulation.

The southern half of the Lower Noatak Lowlands was burned by lightning-caused wildfires in 1977 (the "OTZ NNW 38" fire, 159 plots), 1987 (the "pingo" fire, reburned one plot from 1977), and 2010 (the "Eli River" fire, 37 plots, none of which burned in 1977)(Alaska Interagency Coordination Center 2021). Thus I was able to test the effect of the 1977 and 2010 fires on ice-wedge degradation. The 2010 Eli River fire was predominantly of low severity (MTBS 2021). Severity data are lacking for the 1977 OTZ NNW 38 fire, but other fires in NOAT from 1977 had a range of severities from low to high (Racine, Allen, and Dennis 2006).

Coastal Plain, Bering Land Bridge National Preserve

About half of the Bering Land Bridge National Preserve (BELA) Preserve is an extensive coastal plain where ice-wedge polygons are widespread on the ground between numerous lakes of thermokarst origin (Jorgenson 2001). Very ice-rich Pleistocene "yedoma" sediments occur on this coastal plain and make up much of what Jorgenson (2001) mapped as "Upper Coastal Plain" subsections. In yedoma regions very large syngenetic ice wedges are present in gently sloping uplands between deep thermokarst lakes (Shur et al. 2012). In subsections mapped as "Lower Coastal Plain" (Jorgenson 2001), most of the Pleistocene wedge ice has been lost due to the action of thermokarst, and the surface is covered by shallow thermokarst lakes and sediments from former thermokarst lakes that have drained (Fig. 6) (Jones et al. 2011). Holocene-aged epigenetic ice wedge polygons are widespread in these drained lake basins, especially in older drained-lake basins. (Basin ages estimated by Jones et al. 2012.)

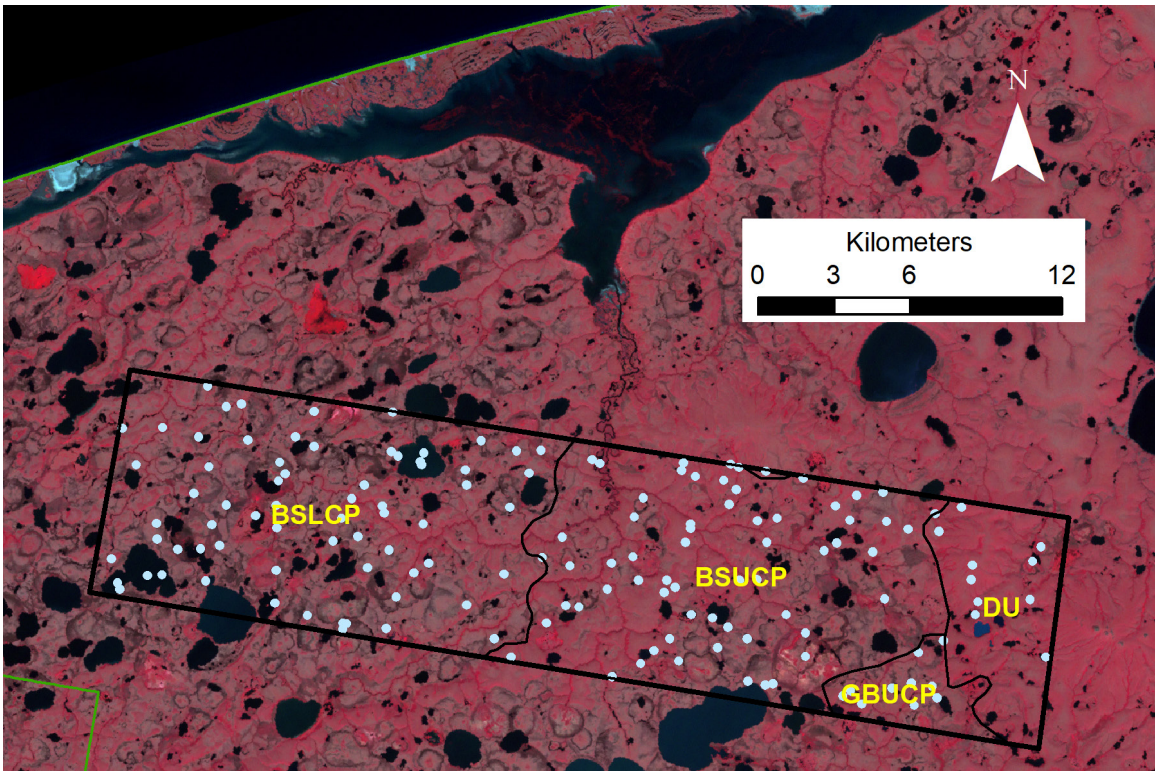


Figure 6. The BELA study area. Dots mark remotely sensed plot locations. Subsections are outlined in black: Bering Straits Lower Coastal Plain (BSLCP), Bering Straits Upper Coastal Plain (BSUCP), Goodhope Bay Upper Coastal Plain (GBUCP), Devil Uplands (DU).

Unlike the previous two study areas, where ice-wedge polygons are limited to a relatively small area and it was reasonable to draw samples from the only polygon-rich subsection in the NPS unit, the polygon-rich BELA coastal plain is so extensive that it would be difficult to obtain and process images across its entirety. Thus, I chose a rectangular 342 km^2 sampling area spanning upper and lower coastal plain subsections and a small area of a third coastal plain subsection, the Devil Uplands (Jorgenson 2001; Fig. 6). Surface materials are peat and lake sediments (from drained thermokarst lakes) on the lower coastal plain, and loess plus volcanic ash deposits on the sloping areas of the upper coastal plains and Devil Uplands. Twenty-four soil pits dug in the area on both drained-lake basins and remnant yedoma as a part of another study (Swanson 2013) on 20-24 July 2013 were frozen at depths of 20-36 cm, in most cases had peat surface soils and water tables near the surface. The vegetation of this study area is herbaceous and low-shrub tundra, varying in wetness from very wet tundra and shallow water emergent vegetation in drained lake basins on the lower coastal plain, to mesic tundra on sloping areas of the upper coastal plains and the Devil Uplands. Dominant plants observed at the 24 sample plots in 2013 were *Sphagnum* sp. mosses and various *Carex* sedge species (especially *C. aquatilis*) in the wettest drained lake basins, while more mesic areas had cottonsedge (*Eriophorum vaginatum*), and low shrubs (*Ledum palustre*, *Vaccinium vitis idaea*, and *Betula nana*). There were no recorded fire perimeters in the BELA study area (Alaska Interagency Coordination Center 2021).

Climate

Long-term climate records are available for Kotzebue, about 175 km west of the KOVA study area, 70 km south of the NOAT study area, and 110 km northeast of the BELA study area. Mean annual air temperatures (MAAT; Fig. 7), which are important in determining the stability of permafrost, rose rather abruptly in 1976-77 and then were relatively stable through 2013. After 2013 MAAT again rose abruptly and record highs were set during the period 2014-2019, which immediately preceded my most recent sampling episode 3 (on satellite images from 2019 and 2020). The sum of thaw degree-days (TDD), which is important in determining the depth of summer thaw, shows similar long-term trends at Kotzebue (Fig. 8): warming in the late 1970s followed by a period of relative stability and then recent renewed warming. The recent increase in TDD appears to have begun earlier than the rise in MAAT, starting with a record value in 2004 that preceded my 2nd sampling episode (2006-2009). Annual precipitation at Kotzebue generally declined from 1950 to 1970 and rose 1970 to 1990 Fig. 9). Since 1990 it has shown considerable year-to-year variation but weak trends.

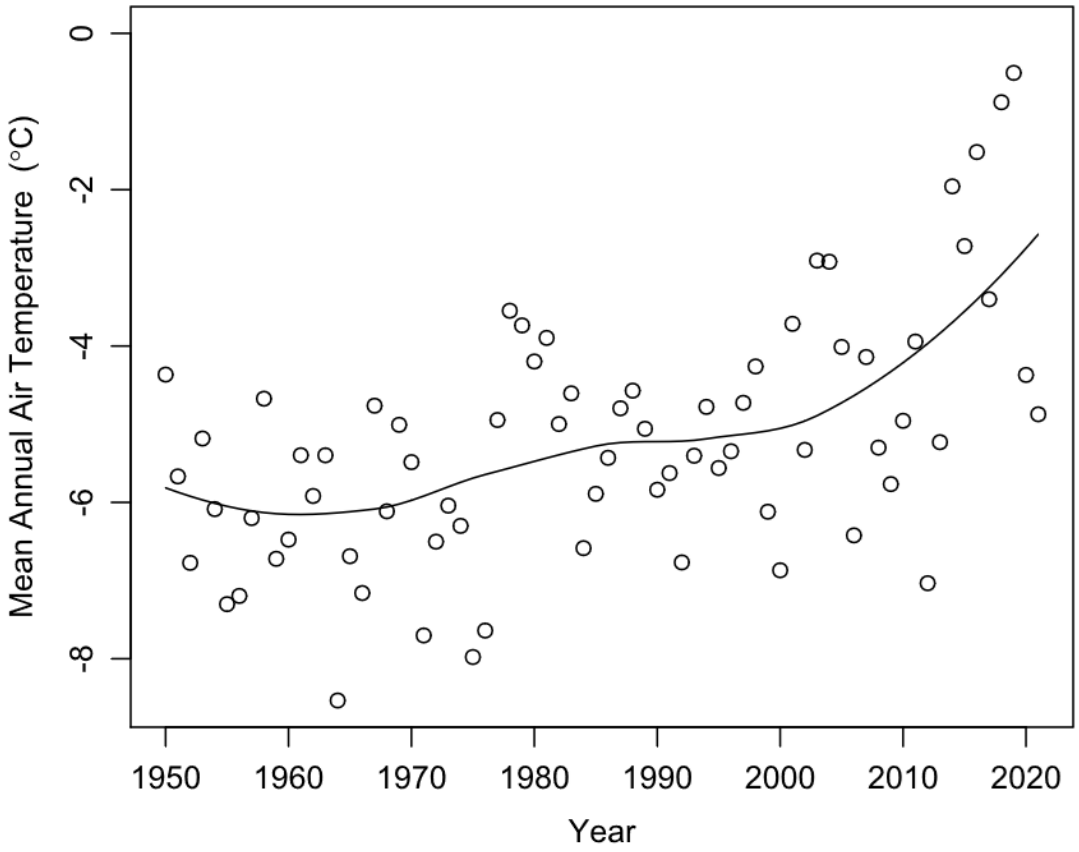


Figure 7. Mean annual air temperature vs. year in Kotzebue, Alaska. Values were computed for hydrologic years (October through September) using monthly means from National Weather Service Data (NOAA Regional Climate Centers 2021). The trendline is a loess curve (span=0.75, degree=2)(R Core Team 2021).

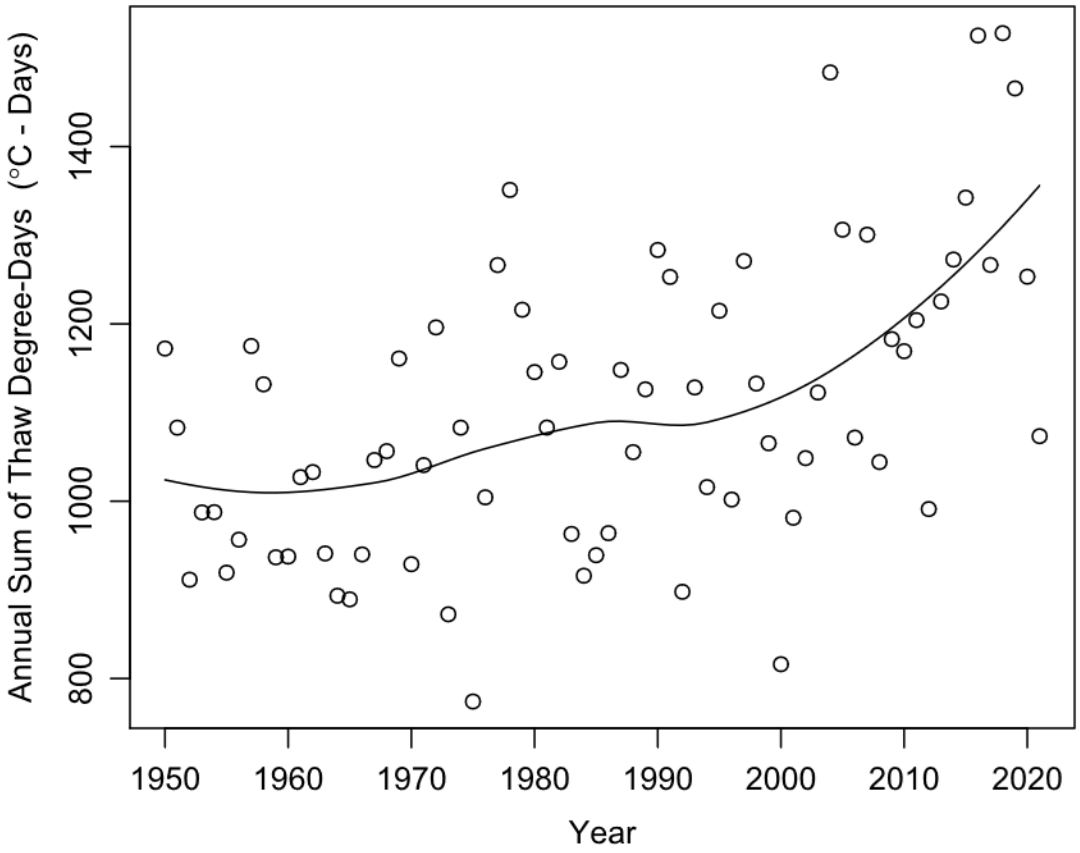


Figure 8. Annual sum of thaw degree-days vs. year in Kotzebue, Alaska. Values were computed for calendar years. The trendline is a loess curve (span=0.75, degree=2)(R Core Team 2021).

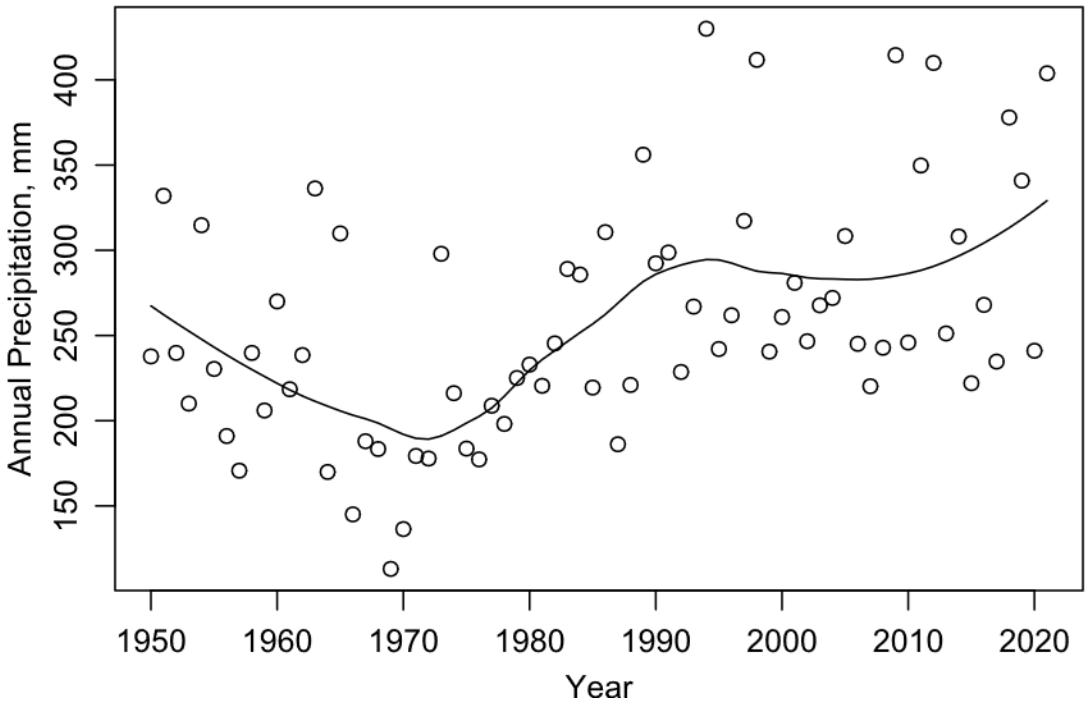


Figure 9. Annual total precipitation in Kotzebue, Alaska. Values were computed for hydrologic years (October through September) using monthly means from National Weather Service Data (NOAA Regional Climate Centers 2021). The trendline is a loess curve (span=0.75, degree=2)(R Core Team 2021).

Analytical Methods

Analytical methods are described in detail by standard operating procedures in (Swanson 2017b) and summarized below. The analysis was based on imagery from three episodes (Table 1.)

Historical Aerial Photograph Preparation

Most of the KOVA and NOAT study areas were covered by panchromatic aerial photographs with film scale of approximately 1:20,000, taken in 1951 or 1952 (U.S. Geological Survey 2018). The exact photo dates are given in Table 1. 1950s-era photos of adequate quality to assess ice wedge condition were not available for the BELA study area. These photos were processed prior to my previous monitoring report (Swanson 2016). Photos were scanned by the US Geological Survey EROS Data Center at 1800 dpi (14 microns). Scans were georeferenced to the IKONOS satellite images (described below) using ArcGIS 10.2 software with a perspective transformation and at least 10 control points per photo. The total root mean square error of each set of control points was less than 1 m, and no control point with greater than 2 m error was accepted. In this region of nearly flat topography, a perspective transformation yielded acceptable results without orthorectification. The corrected photos were resampled to 1 m resolution (matching the IKONOS imagery) by bilinear interpolation. The corrected photos were joined into a mosaic where overlap areas were displayed using the photo with the nearest center. I corrected all of the available photos, which had approximately 60% overlap, so sampling was restricted to near the center of each photo, where spatial distortion and vignetting (the tendency for corners of photos to be darker) were minimized.

Table 1. Dates of imagery used in this study[A]

Study Area	Episode 1: 1951-52 Aerial Photographs[B]	Episode 2: 2006-2009 IKONOS Satellite images[C]	Episode 3: 2019-20 Worldview-2 Satellite images[D]
BELA	• None	• 20080807	• 20190525 • 20190604 • 20190616
KOVA	• 19510825 • 19510826 • 19520827	• 20060920 • 20070810 • 20090930	• 20200621 • 20190707
NOAT	• 19510715	• 20060904 • 20070703 • 20070706 • 20080708	• 20190613

[A]YYYYMMDD format

[B]Panchromatic, scale 1:20,000 scanned at 1800 dpi (14 microns), equivalent to about 0.3 m resolution, and resampled to 1 m

[C]Panchromatic raster reconstructed from 1 m pansharpened multispectral data

[D]Panchromatic 0.46 m resolution, resampled to 1 m

IKONOS Image Preparation

NPS has nearly complete IKONOS satellite image coverage (Satellite Imaging Corporation 2022a) of the northern Alaska National Park units, acquired in 2006 through 2009. Exact image dates are given in Table 1. This is 4-band color-infrared imagery with 4-m resolution, pan-sharpened to 1 m resolution. Images for the KOVA and NOAT study areas were processed prior to my previous monitoring report (Swanson 2016). Images were orthorectified using the manufacturer's satellite parameters and the 60 m National Elevation Dataset digital elevation model. The original panchromatic images used to create these pan-sharpened images were not available, so I re-created an 8-bit (256 illumination levels) panchromatic satellite images by combining the red, green, and blue bands with equal weights to match the 1950s panchromatic aerial photographs. Some plots were not available to sample on the IKONOS images due to clouds, mainly in the KOVA study area.

I orthorectified the IKONOS images for the BELA study area in 2021 using an updated DEM (USGS 2015) and reconstructed the panchromatic images using all 4 bands to better match the newer Worldview-2 images. In BELA I also corrected the georeferencing of the IKONOS images to the Worldview-2 satellite images (described below) using ArcGIS 10.7 software with an affine transformation and at least 10 control points per image. The total root mean square error of each set of control points was less than 1 m.

Worldview-2 Image Preparation

Cloud-free, orthocorrected, panchromatic Worldview-2 images (0.46 m resolution)(Satellite Imaging Corporation 2022b) from 2019 were available for the BELA and NOAT study areas, while images from both 2019 and 2020 were needed to cover the KOVA study area. To match existing images from the previous monitoring iteration (Swanson 2016), I georeferenced the Worldview-2 images for KOVA and NOAT to the IKONOS images, using ArcGIS 10.7 software with an affine transformation and at least 10 control points per image. The total root mean square error of each set of control points was less than 1 m. Since this legacy of completed work was not available for the BELA study area, I chose to make the newer Worldview-2 images be the standard to which the others would be registered, and thus georeferenced the IKONOS to it as described above. Worldivew-2 images were resampled to 1 m resolution using bilinear interpolation to match all other image sources.

Plot Establishment

Within each study area I generated 400 randomly located circular 1-ha plots (radius 56.42 m) within each study area's constraining feature. In the KOVA study area of the constraining feature for random plots was the 141.9 km^2 Ahnewetut Wetlands Subsection (Swanson 2001)(Table 2). I sampled the plots in random order, discarding one with extensive tree shadows (which would be mistakenly mapped as water). I continued until I had sampled 335 plots, of which 301 were free of clouds or cloud shadows on the IKONOS images (other dates had less cloud cover). Ninety-one plots had identifiable ice-wedge polygons as of 2019-20 (Table 2).

In the NOAT study area, all image dates were cloud-free and lacked significant tree shadows. The constraining feature for the random plots (the Lower Noatak Lowlands Subsection; (Jorgenson, Swanson, and Macander 2001) was clipped to the limits of available 1950s photos and the NOAT boundary. Here I sampled 300 plots on all dates, of which 136 had identifiable ice-wedge polygons as of 2019.

In BELA study area, ice-wedge polygons cover a larger proportion of the surface here than in the other study areas. After sampling the first 151 plots I had already identified 109 with ice-wedge polygons, a sample comparable to the other two study areas (n = 91 and 136). In the interest of time savings I discontinued further sampling.

Table 2. Plot Properties

Study Area	Constraining Feature Area[A] (km^2)	Plots Sampled[B] (1) Photos 1950-51	(2) IKONOS 2006-09	(3) WV-2 2019-20	Count of Plots with Ice wedges	Count of Ice-wedge centers	Area of Ice wedge Zones (% of plot area)
BELA	342	0	148	151	109	1634	24
KOVA	142	333	301	335	91	1426	8
NOAT	267	300	300	300	136	3260	22

[A]Area of constraining feature inside of which random plots were located

[B]The number of plots varied because clouds obscured some of the plots in some years

Identification of Ice-Wedge Polygon Zones

Within each plot I digitized a point at the center of every ice-wedge polygon that was visible on any image date. I also digitized ice-wedge polygon center points outside but within 30 m of the plot boundaries. The area encompassed by ice-wedge polygons within the plots was then outlined using the ArcGIS "Aggregate Points" geoprocessing tool, which connected the ice-wedge polygons centers closer than a chosen distance (30 m) and created a GIS polygon from the outermost of these lines. The resulting areas were clipped to the circular plot boundaries and are referred to as "ice-wedge polygon zones". Many of the 1-ha plots were only partly occupied by polygons (or lacked them entirely). Thus the plots represent samples of different sizes, and I chose to aggregate them for analysis, treating them as a single sub-area that is representative of the whole.

Mapping of Ice-Wedge Polygon Pits and Ponds

Water-filled pits and ponds were mapped by thresholding the panchromatic images (Jorgenson, Shur, and Pullman 2006; Liljedahl et al. 2016). Water bodies are the main dark-colored feature on the images, and thus a map of water bodies can be made by choosing a threshold pixel darkness and classifying all darker pixels as "water" and lighter pixels as "land". Thresholds were chosen manually for each image, with special attention to the ice-wedge zones and their vicinities; obvious water bodies outside the zones were also helpful as guides. The resulting binary raster maps (water vs. land) were clipped to the ice-wedge polygon zone boundaries within the plots.

Water bodies within the ice-wedge zones are shallow and often have gently sloping margins with emergent vegetation; this makes differentiation of land and water difficult. As a result, a range of reasonable choices of thresholds can yield estimates of water area in ice-wedge zones that vary by a factor of almost two. For this reason, I chose the threshold for each image to produce what I judged subjectively to be the best possible map of water bodies, but I did not rely on the simple area of water to determine if ice wedges had degraded. My analysis is based on position of water bodies relative to polygon centers and not the area of water alone, because the location of water bodies relative to polygon centers and margins was much less sensitive to the choice of thresholds.

Compute and Analyze the Position Index of Water Pixels

I computed the distance from the center of each 1 m^2 water pixel to the two closest ice-wedge polygon centers using the ArcGIS "Generate Near Table" geoprocessing tool. The position index of each water pixel was then computed by the formula $2a/(a + b)$, where a is the distance from the center of the pixel to the closest ice-wedge polygon center and b is the distance to the second closest ice-wedge polygon center (Fig. 10). This index is known to community ecologists as the Sørenson distance index (McCune, Grace, and Urban 2002) and it ranges from near 0 at the polygon centers (where a is small and b relatively large) to near 1 along polygon boundaries (where a and b are approximately equal). The index was also computed for 10,000 random points in the ice-wedge zones of the KOVA and NOAT study areas. In both study areas the distance indices for the 10,000 random points were 0.56, 0.75, and 0.89 for the 25th, 50th, and 75th quantiles, respectively. These quantile breaks were used to define "quarter sectors" of the polygons. Thus all water pixels with indices between 0 and 0.56 were considered part of quarter sector 1, the innermost one-fourth of the polygons; pixels with an index of 0.56 to 0.75 were assigned to quarter sector 2 (just outside sector 1), and so on.

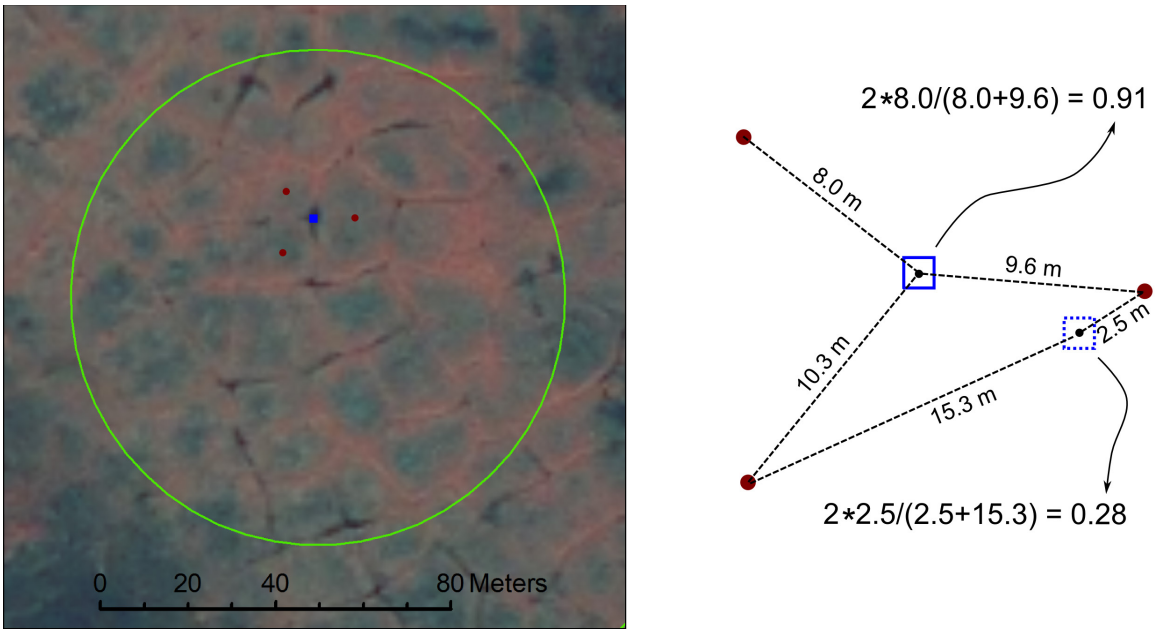


Figure 10. Computation of the water pixel position index. On the left is an example plot (plot 63 in the KOVA study area) with an example water pixel in blue on the polygon margins and three neighboring ice-wedge polygon centers. On the right, these features are magnified and the distance index is computed for this pixel (solid blue square) and a hypothetical pixel near one of the polygon centers (dotted blue square). The solid blue pixel near the polygon margins has a distance index of 0.91, indicating that it is on the polygon margins, while the dashed pixel near the right-most polygon center has an index of 0.28, indicating that it is near the polygon center.

The differences in the distribution of distance indices for water pixels between the two image dates, and between plots inside vs. outside the fire perimeter the NOAT study area, were tested using the Wilcoxon Rank Sum test with continuity correction (the "wilcox.test" function in R statistical software; (R Core Team 2021).

Visual Assessment of Ice-Wedge Polygons

I also made a visual classification of polygon type on each 1-ha plot, and a visual assessment of the presence or absence of water-filled pits along polygon margins in the plot. The polygons on each plot were classified as low-centered (more than two-thirds of polygons had dark-colored centers), high-centered (more than two-thirds of polygons had light-colored centers), or mixed (both dark- and light-centered polygons were present, neither dominant; or polygons generally flat and high vs. low classes were difficult to discern). Water-filled marginal pits were considered "present" if any were found along polygon margins in the 1-ha plot. I did not attempt a significance test of the visual classification data, because the plots are not each equivalent samples from the population: the area of the ice wedge zones within the plots varies widely, from not present to the full 1 ha.

Visual Assessment of ice-wedge drainage channels

Our current monitoring protocol emphasizes the abundance of ice-wedge marginal ponds. An important related feature of wedge degradation is the appearance of new drainage channels that form by linking of adjacent wedge ponds, and associated thermal erosion. I made a rapid survey of the

three study areas for newly formed drainage channels along a systematic grid of 1 X 2 km rectangular cells at a viewing scale of 1:5,000. I compared the most recent Worldview-2 2019-2020 images with the IKONOS 2006-2009 images and digitized as a line feature any newly observed drainage channels.

Results

In the BELA study area, the plots contained dominantly .low-center polygons (Fig. 11). The proportion of plots with marginal ponds increased somewhat between the two sampling episodes, from 22% of plots on the 2008 IKONOS images to 29% of plots on the 2019 Worldview-2 images; most of the increase occurring in plots with low-center polygons (Table 3). However, the overall distribution of water across the different sectors of the ice-edge polygons was very similar on the 2008 and 2019 images (Fig. 12). (Recall that "the proportion of plots with marginal ponds" refers to plots with any marginal ponds present, and does not indicate how much of the water was at the margins.) More water was located in the polygon center sector (sector 1 in Fig. 12) than in the others, as would be expected in an area dominated by low-center polygons. The median distance index of water pixels from polygon centers did not change between the two sample episodes (0.66 in both; Table 3). The Wilcoxon rank-sum test for the difference in distance index between the two episodes was nonsignificant, $p = 0.998$ (Table 4).

Table 3. Summary of ice-wedge polygon water mapping

Study Area	Image Years	Water Area, %	Proportion of Plots with Marginal Ponds, %
BELA	2008	7.2	22
	2019	8.0	29
KOVA	1951-52	1.2	16
	2006-09	1.2	59
	2019-20	2.7	71
NOAT	1951	0.7	30
	2006-08	0.7	49
	2019	3.6	44

Table 4. Summary of Water Distance Indices by Study Area and Sampling Episode

	Median Water Distance Index by Episode: Years			Wilcoxon Test p-value by Episode vs. Episode		
Study Area	**1: 1951-52**	**2: 2006-2009**	**2: 2019-20**	**1 vs. 2**	**1 vs. 3**	**2 vs. 3**
BELA	No Data	0.66	0.66	No Data	No Data	0.988
KOVA	0.67	0.85	0.82	0.000	0.000	0.185
NOAT	0.75	0.80	0.71	0.111	0.312	0.000

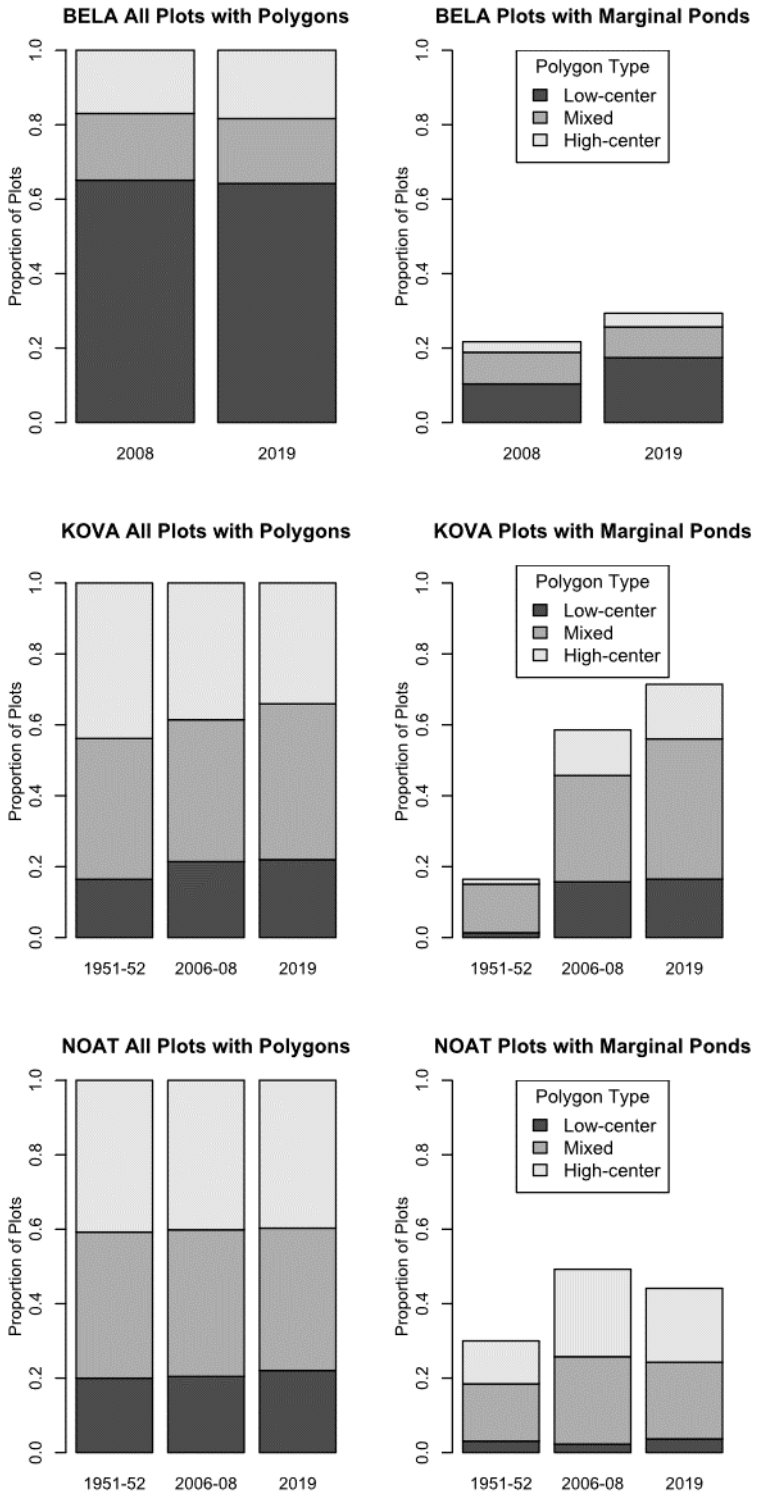


Figure 11. Summary of ice-wedge polygon types from visual assessment.

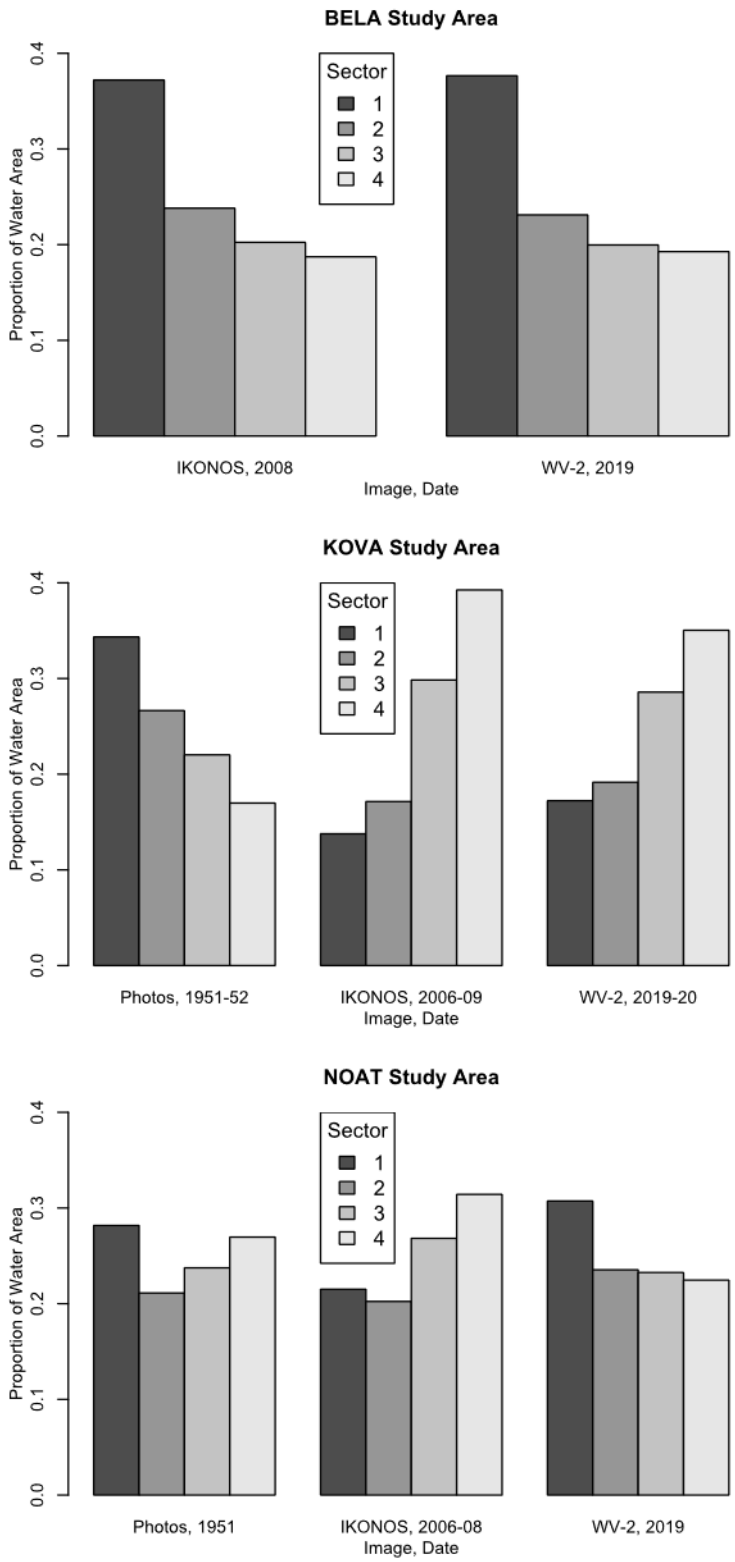


Figure 12. Water distribution by ice-wedge polygon sector. The four sectors are concentric zones, each occupying one-fourth of the area of individual ice-wedge polygons. Sector 1 is the center one-fourth of all polygons, while sector 4 is the outermost one-fourth of all polygons (i.e. near the polygon margins).

In the KOVA study area, most plots had high-center or mixed polygons in all 3 sampling episodes (Fig. 10). The proportion of plots with marginal ponds jumped from 16% on the 1950s photos to 59% on the 2006-09 IKONOS images and 71% on the 2019-20 Worldview-2 images. All polygon types showed increases on marginal ponds. Water was concentrated in polygon centers in the 1951-52 sample (34% of water pixels were in sector 1), but this changed abruptly in the subsequent sampling episodes to be less than 20% in the center (sector 1) and more than 35% in the margins (sector 4). The change occurred mainly between the 1951-52 and 2006-09 sampling episodes, with little change thereafter. The change in median water distance index changed significantly between the 1951-52 and 2006-09 (0.67 to 0.85, Wilcoxon test $p < 0.001$) but not between 2006-09 and 2019-20 (0.85 to 0.82, Wilcoxon test $p = 0.185$). An example plot from the KOVA study area (Fig. 13) shows ice-wedge polygon marginal ponds that formed between 1952 and 2007, and possibly enlarged further between 2007 and 2020.

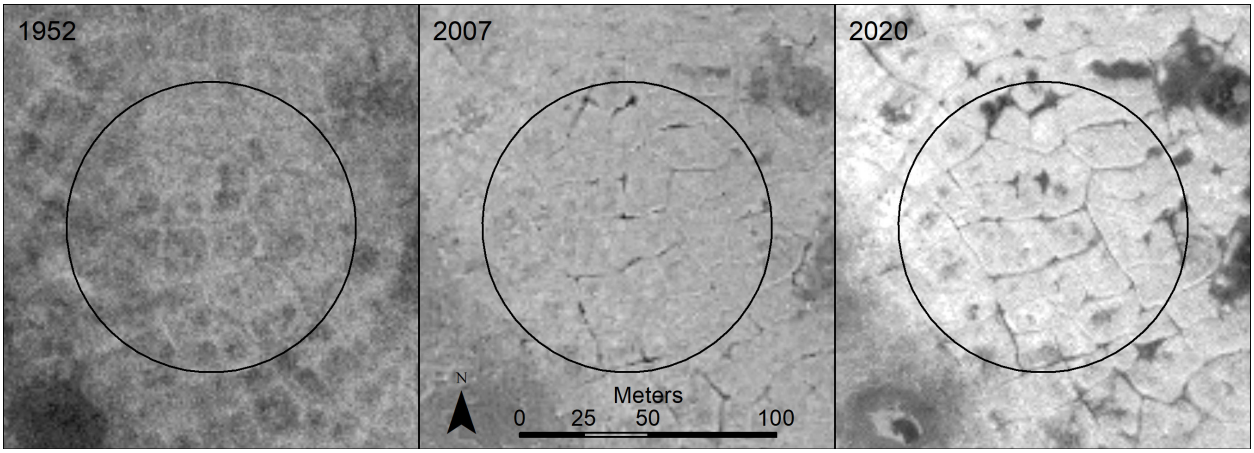


Figure 13. History of KOVA study area plot 63. Ice-wedge polygon marginal ponds formed between 1952 and 2007, and enlarged further between 2007 and 2020. The similarity in shape and location of the ponds in 2007 and 2020 suggests their enlargement may have been due to wetter conditions in the latter year rather than (or in addition to) continued thaw subsidence.

The NOAT study area was also dominated by mixed and high-center polygons. The proportion of plots with polygon-marginal ponds increased from 30% in 1951 to 49% in 2006-08 (with most of the increase occurring in mixed and high-center polygon plots) and then dropped slightly to 44% in 2019. The distribution of water may have shifted somewhat from centers to margins between the 1951 and 2006-08 episodes, but the shift was less marked than at KOVA and the change in the median water distance index from 0.75 to 0.80 (Table 3) was not highly significant (Wilcoxon test $p = 0.111$). In the 2019 sampling episode the water distribution appeared to shift back toward the centers: the median value of 0.71 in 2019 was significantly lower than in 2006-08 ($p = 0.000$) but not 1951 ($p = 0.312$). An example plot from the NOAT study area (Fig. 14) shows ice-wedge marginal pits present at all three sample episodes.

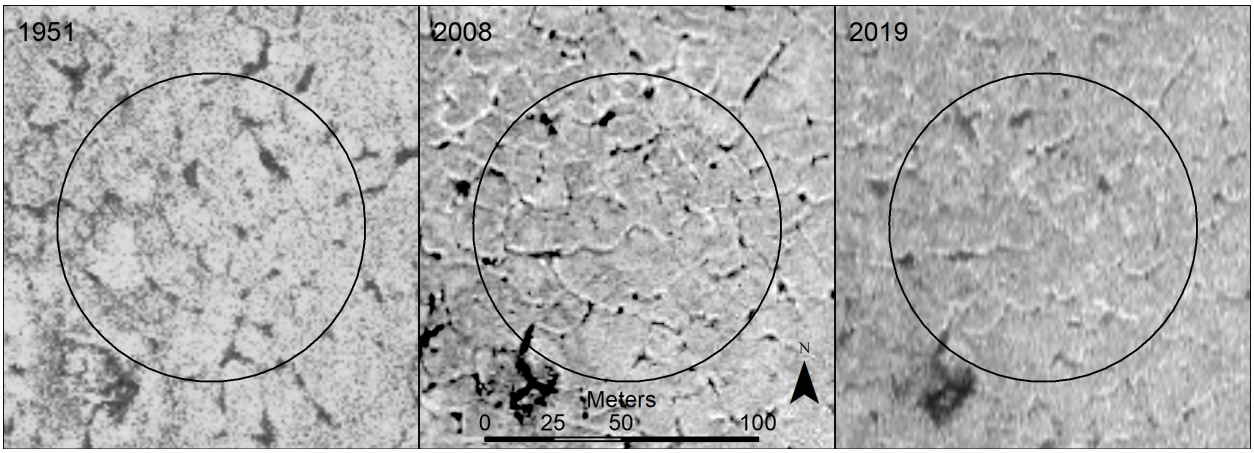


Figure 14. History of NOAT study area plot 26. Ice-wedge marginal pits were present at all three sample episodes. Some pits present in 1951 became less prominent and some new ones formed by 2008. There was little additional change by 2019.

The fires in NOAT had weak effects on the distribution of water in ice-wedge polygons. The median water distance index for plots within the 1977 fire was slightly but significantly lower (by Wilcoxon rank-sum test, Table 5) in episode 3 than the preceding two episodes, meaning that slightly more water was found in polygon centers after the fire than before, i.e. wedge degradation did not occur. In the 2010 fire perimeter the water distribution index was also slightly lower in the last sampling episode than in either preceding episode, but not significantly so (Table 5).

Table 5. Water Distance Indices and Fires in the NOAT study area

		Median Water Distance Index by Episode: Years			Wilcoxon Test p-value by Episode vs. Episode		
Treatment	**Plots**	**1: 1951-52**	**2: 2006-08**	**3: 2019**	**1 vs. 2**	**1 vs. 3**	**2 vs. 3**
No burn	103	0.71	0.78	0.73	0.181	0.704	0.008
1977 burn	159	0.76	0.82	0.69	0.330	0.045	0.003
2010 burn	37	0.91	0.87	0.86	0.210	0.211	0.289

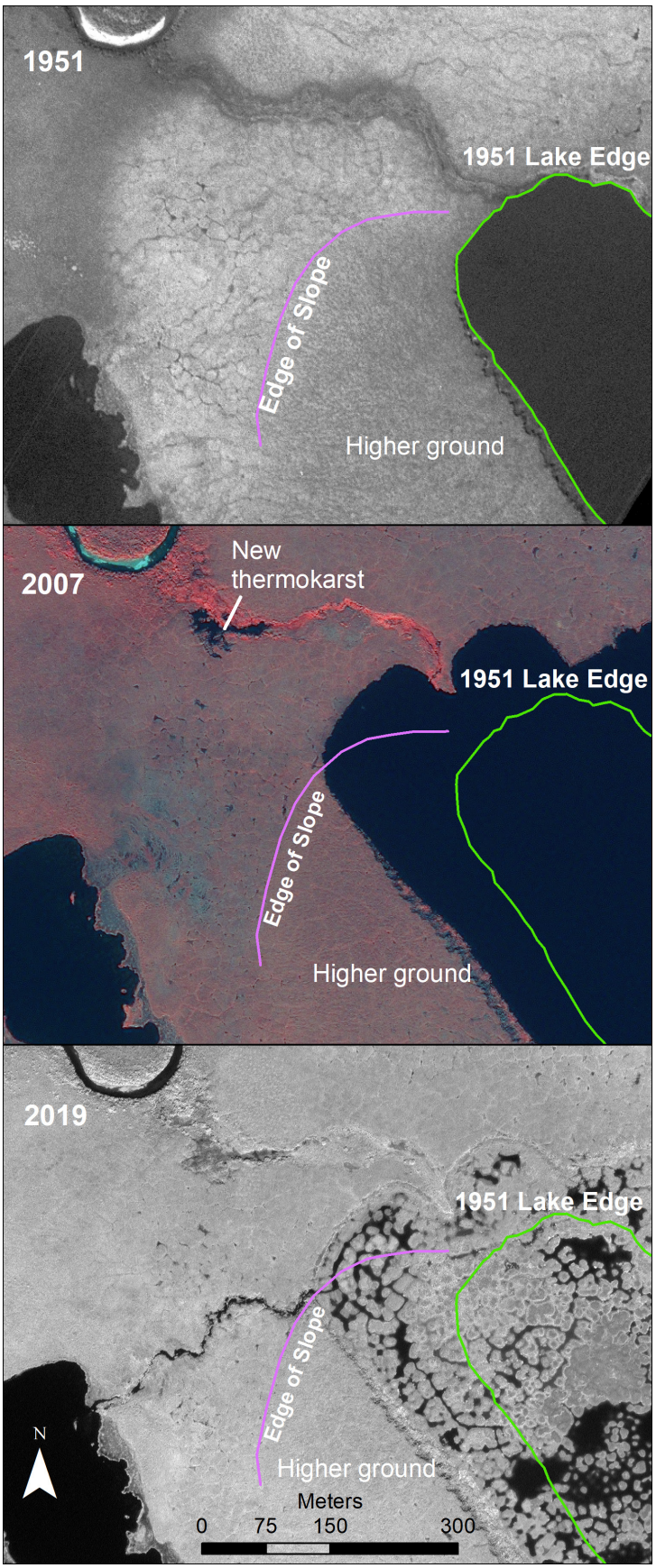
The visual assessment of new drainages channels that formed between the IKONOS 2006-09 and WV-2 2019-2020 images showed that new channels formed, even in the absence of major changes in marginal pond area. The length of new channels was quite similar between the study areas at 9 m km^{-2} (KOVA and NOAT) and 12 m km^{-2} (BELA; Table 6). The most dramatic effect of new channel formation is lake drainage, which was noted in one location in the NOAT study area (Fig. 15). Here a new channel formed, flowing to the southwest across a field of ice wedges that was visibly degraded on both the 1951 aerial photograph and the 2007 IKONOS image. The lakeshore advanced by thermokarst/thermal erosion between 1951 and 2007; this placed the shoreline in contact with the field of degraded wedges west of the lake, allowing it to find a new channel that thermo-eroded and deepened, allowing the lake to drain by 2019. Surprisingly, the lake did not drain through the pre-

existing lake outlet to the northwest, in spite of the active thermokarst that occurred along it (Fig. 15).

Table 6. Dimensions of new drainage channels observed between IKONOS 2006-09 and WV-2 2019-2020 images

Study Area	Count	Total Length (m)	Length per unit area (m km^{-2})
BELA	21	4035	11.8
KOVA	13	1305	9.2
NOAT	7	2483	9.3

Figure 15 (following page). Channel formation and lake drainage along degraded ice wedges in NOAT. This area had scattered small thermokarst pits due to ice-wedge degradation on the 1951 aerial photograph (upper) that changed little through the 2007 IKONOS (center) and 2019 (lower) Worldview-2 images. More substantial thermokarst is visible in 2007 in the form of an intricate pond along the original drainage channel leading from the north end of the lake (the channel has bright red color due to shrubs). This thermokarst surprisingly did not visibly affect the lake level. However, north- and westward advance of the lakeshore edge after 1951 opened up a drainage pathway through degraded ice wedges north and west of the higher ground west of the lake, and this allowed the lake to drain between 2007 and 2019. View is centered near longitude -162.520, latitude 67.550.


1951
1951 Lake Edge
Edge of Slope
Higher ground
2007
New
thermokarst
1951 Lake Edge
Edge of Slope
Higher ground
2019
1951 Lake Edge
Edge of Slope
Higher ground
N
Meters
0
75
150
300

Discussion and Conclusions

This third episode of sampling (image dates 2019-2020) for ice-wedge degradation revealed relatively minor changes from the second episode (image dates 2006-2009). The best evidence of change was actually for slight recovery of ice wedges in the NOAT study area. This is somewhat surprising given the record warm temperatures that occurred between the second and third sampling episodes. Apparently the recent warming did not force the ice wedges to cross any thresholds that would trigger immediate and widespread visible changes. A previous cycle of ice-wedge degradation and recovery typically creates a thick protective layer of ice-poor material (the "intermediate layer") over any remaining parts of ice wedges (Jorgenson et al. 2015; Kanevskiy et al. 2017). A thick, new, and ice-poor intermediate layer can protect quite effectively against thermokarst, at least until sufficient time has passed to accumulate new ice in the intermediate layer (Kanevskiy et al. 2017). This presumed ice-poor layer apparently was sufficient to protect the ice wedges in my study areas from the unusual warmth that began in 2014. It is also possible that insufficient time has elapsed since the recent onset of warmer temperatures in 2014, though in some circumstances just a few years are sufficient to produce new ice-wedge marginal ponds (Kanevskiy et al. 2017). Precipitation trends from 1990-2020 were weak, suggesting that a change in precipitation did not facilitate ice-wedge stability by somehow offsetting the rise in temperatures.

New drainage channels continued to form by linkage of pits from previous ice-wedge degradation, and in one case this led to drainage of a lake. Thus earlier ice-wedge degradation paved the way for more dramatic changes years later, even in the absence of much new wedge degradation.

The NOAT study area was affected by wildfires in 1977 and 2010, and comparison of burned to unburned areas in subsequent sampling episodes failed to show significant new ice-wedge degradation brought about by these fires. This lack of fire effects stands in contrast to the findings of Jones et al. (2015) for the Anaktuvuk River fire on the North Slope of Alaska, where significant post-fire thermokarst was observed. The difference could be due to differing burn severity: the Anaktuvuk River fire was of high severity after exceptionally warm and dry weather (Kolden and Rogan 2013; Jones et al. 2009), while the 2010 NOAT study area fire was of low severity (MTBS 2021); the severity of the 1977 fire was unknown. In addition, the same ice-poor intermediate layer that apparently protected the wedges from degrading during the post-2013 warm weather could also have help protect it from degradation after the wildfires.

Literature Cited

Alaska Interagency Coordination Center. 2021. “AICC Predictive Services - Maps/Imagery/Geospatial.” *AICC Predictive Services - Maps/Imagery/Geospatial*. https://fire.ak.blm.gov/predsvcs/maps.php.

Cleland, D. T., P. E. Avers, W. H. McNab, M. E. Jensen, R. G. Bailey, T. King, and W. E. Russell. 1997. “National Hierarchical Framework of Ecological Units.” In *Ecosystem Management Applications for Sustainable Forest and Wildlife Resources*, edited by M. S. Boyce and A. Haney, 181–200. New Haven, CT: Yale University.

Cohen, K. M., S. C. Finney, P. L. Gibbard, and J.-X. Fan. 2013. “The ICS International Chronostratigraphic Chart.” *Episodes* 36 (3): 199–204. http://www.episodes.org/index.php/epi/article/view/59399.

Czudek, T., and J. Demek. 1970. “Thermokarst in Siberia and Its Influence on the Development of Lowland Relief.” *Quaternary Research* 1 (1): 103–120. http://www.sciencedirect.com/science/article/pii/003358947090013X.

Hamilton, T. D. 2010. “Surficial Geologic Map of the Noatak National Preserve, Alaska. Scientific Investigations Map 3036.” Denver, Colorado: US Department of the Interior, Geological Survey. http://pubs.usgs.gov/sim/3036/.

Jones, B. M., G. Grosse, C. D. Arp, M. C. Jones, K. M. Walter Anthony, and V. E. Romanovsky. 2011. “Modern Thermokarst Lake Dynamics in the Continuous Permafrost Zone, Northern Seward Peninsula, Alaska.” *Journal of Geophysical Research: Biogeosciences (2005–2012)* 116 (G2): G00M03. doi:10.1029/2011JG001666.

Jones, B. M., G. Grosse, C. D. Arp, E. Miller, L. Liu, D. J. Hayes, and C. F. Larsen. 2015. “Recent Arctic Tundra Fire Initiates Widespread Thermokarst Development.” *Scientific Reports* 5: 15865. doi:10.1038/srep15865.

Jones, B. M., C. A. Kolden, R. Jandt, J. T. Abatzoglou, F. Urban, and C. D. Arp. 2009. “Fire Behavior, Weather, and Burn Severity of the 2007 Anaktuvuk River Tundra Fire, North Slope, Alaska.” *Arctic, Antarctic, and Alpine Research* 41 (3): 309–316. http://www.bioone.org/doi/abs/10.1657/1938-4246-41.3.309.

Jones, M. C., G. Grosse, B. M. Jones, and K. Walter Anthony. 2012. “Peat Accumulation in Drained Thermokarst Lake Basins in Continuous, Ice-Rich Permafrost, Northern Seward Peninsula, Alaska.” *Journal of Geophysical Research: Biogeosciences (2005–2012)* 117 (G2): G00M07. doi:10.1029/2011JG001766.

Jorgenson, M. T. 2001. “Ecological Subsections of Bering Land Bridge National Preserve.” Anchorage, Alaska: Inventory and Monitoring Program, National Park Service, Alaska Region.

https://irma.nps.gov/App/Reference/DownloadDigitalFile?code=418816&file=BELA_Ecological Subsections.pdf.

Jorgenson, M. T., M. Kanevskiy, Y. Shur, N. Moskalenko, D. R. N. Brown, K. Wickland, R. Striegl, and J. Koch. 2015. “Role of Ground Ice Dynamics and Ecological Feedbacks in Recent Ice Wedge Degradation and Stabilization.” *Journal of Geophysical Research: Earth Surface* 120 (11): 2280–2297. http://onlinelibrary.wiley.com/doi/10.1002/2015JF003602/full.

Jorgenson, M. Torre, Y. L. Shur, and E. R. Pullman. 2006. “Abrupt Increase in Permafrost Degradation in Arctic Alaska.” *Geophysical Research Letters* 33 (2). http://onlinelibrary.wiley.com/doi/10.1029/2005GL024960/pdf.

Jorgenson, M. Torre, D. K. Swanson, and M. Macander. 2001. “Landscape-Level Mapping of Ecological Units for the Noatak National Preserve, Alaska.” Anchorage, Alaska: Inventory and Monitoring Program, National Park Service, Alaska Region. https://irma.nps.gov/App/Reference/DownloadDigitalFile?code=419154&file=NOAT_EcologicalSubsections.pdf.

Jorgenson, M. Torre, K. Yoshikawa, M. Kanevskiy, Y. Shur, V. Romanovsky, S. Marchenko, G. Grosse, J. Brown, and B. Jones. 2008. “Permafrost Characteristics of Alaska.” Fairbanks, Alaska: Institute of Northern Engineering, University of Alaska Fairbanks. http://www.cryosphericconnection.org/resources/alaska_permafrost_map_dec2008.pdf.

Kanevskiy, M., Y. Shur, T. Jorgenson, D. R. Brown, N. Moskalenko, J. Brown, D. A. Walker, M. K. Raynolds, and M. Buchhorn. 2017. “Degradation and Stabilization of Ice Wedges: Implications for Assessing Risk of Thermokarst in Northern Alaska.” *Geomorphology* 297: 20–42.

Kolden, C. A., and J. Rogan. 2013. “Mapping Wildfire Burn Severity in the Arctic Tundra from Downsampled MODIS Data.” *Arctic, Antarctic, and Alpine Research* 45 (1). Taylor & Francis: 64–76. https://www.tandfonline.com/doi/full/10.1657/1938-4246-45.1.64.

Lachenbruch, A. H. 1963. “Contraction Theory of Ice-Wedge Polygons: A Qualitative Discussion In.” In *Proceedings, Permafrost International Conference:*, 63–71. Washington, D.C.: National Academy of Sciences, National Research Council. http://www.arlis.org/docs/vol1/ICOP/.

Leffingwell, E. de K. 1915. “Ground-Ice Wedges: The Dominant Form of Ground-Ice on the North Coast of Alaska.” *The Journal of Geology* 23 (7): 635–654. http://www.jstor.org/stable/30062549.

Liljedahl, A. K., J. Boike, R. P. Daanen, A. N. Fedorov, G. V. Frost, G. Grosse, L. D. Hinzman, et al. 2016. “Pan-Arctic Ice-Wedge Degradation in Warming Permafrost and Its Influence on Tundra Hydrology.” *Nature Geoscience* 9: 312–18. doi:10.1038/NGEO2674.

Mann, D. H., P. A. Heiser, and B. P. Finney. 2002. “Holocene History of the Great Kobuk Sand Dunes, Northwestern Alaska.” *Quaternary Science Reviews* 21 (4): 709–731. http://www.sciencedirect.com/science/article/pii/S0277379101001202.

McCune, B., J. B. Grace, and D. L. Urban. 2002. *Analysis of Ecological Communities*. Vol. 28. Gleneden Beach (OR): MjM software design. http://www.researchgate.net/profile/James_Grace/publication/216769990_Analysis_of_ecological_communities/links/0a85e5318e69b2ae7f000000.pdf.

MTBS. 2021. "MTBS." *Monitoring Trends in Burn Severity*. www.mtbs.gov.

Necsoiu, M., C. L. Dinwiddie, G. R. Walter, A. Larsen, and S. A. Stothoff. 2013. "Multi-Temporal Image Analysis of Historical Aerial Photographs and Recent Satellite Imagery Reveals Evolution of Water Body Surface Area and Polygonal Terrain Morphology in Kobuk Valley National Park, Alaska." *Environmental Research Letters* 8 (2): 025007. http://iopscience.iop.org/article/10.1088/1748-9326/8/2/025007/meta.

NOAA Regional Climate Centers. 2021. "XmACIS2." *XmACIS2*. http://xmacis.rcc-acis.org/.

Péwé, T. L. 1975. "Quaternary Geology of Alaska." US Government Printing Office. https://pubs.er.usgs.gov/publication/pp835.

R Core Team. 2021. *R: A Language and Environment for Statistical Computing* (version 4.0.5). Vienna, Austria: R Foundation for Statistical Computing. https://www.R-project.org/.

Racine, C., J. L. Allen, and J. G. Dennis. 2006. "Long-Term Monitoring of Vegetation Change Following Tundra Fires in Noatak National Preserve, Alaska." Natural Resource Technical Report NPS/AKRARCN/NRTR-2006/02. Fairbanks, Alaska: Arctic Network of Parks Inventory and Monitoring Program, National Park Service, Alaska Region. https://irma.nps.gov/DataStore/Reference/Profile/662768.

Satellite Imaging Corporation. 2022a. "IKONOS Satellite Sensor." *IKONOS Satellite Sensor*. http://www.satimagingcorp.com/satellite-sensors/ikonos/.

———. 2022b. "Worldview-2 Satellite Sensor." *Worldview-2 Satellite Sensor*. http://www.satimagingcorp.com/satellite-sensors/worldview-2/.

Shur, Y., M. Kanevskiy, T. Jorgenson, M. Dillon, E. Stephani, M. Bray, and D. Fortier. 2012. "Permafrost Degradation and Thaw Settlement under Lakes in Yedoma Environment." In *Proceedings of the Tenth International Conference on Permafrost*, 1:25–29. Salekhard, Russia. https://ipa.arcticportal.org/meetings/international-conferences.

Swanson, D. K. 2001. "Ecological Units of Kobuk Valley National Park, Alaska." Anchorage, Alaska: Inventory and Monitoring Program, National Park Service, Alaska Region. https://irma.nps.gov/App/Reference/Profile/584437.

———. 2013. "Vegetation Sampling in the Arctic Inventory and Monitoring Network, 2013 Progress Report." Natural Resource Data Series NPS/ARCN/NRDS—2013/580. Fort Collins, Colorado: National Park Service. https://irma.nps.gov/App/Reference/Profile/2204497.

———. 2016. “Stability of Ice-Wedge Polygons in Kobuk Valley National Park and the Noatak National Preserve, 1951-2009.” Natural Resource Report NPS/ARCN/NRR—2016/1248. Fort Collins, Colorado: National Park Service. https://irma.nps.gov/DataStore/Reference/Profile/2230516.

———. 2017a. “Permafrost Monitoring Protocol for the Arctic Network: Narrative.” Natural Resource Report NPS/ARCN/NRR-2017/1396. Fort Collins, Colorado: National Park Service. https://irma.nps.gov/DataStore/Reference/Profile/2238783.

———. 2017b. “Permafrost Monitoring Protocol for the Arctic Network: Standard Operating Procedures.” Natural Resource Report NPS/ARCN/NRR-2017/1397. Fort Collins, Colorado: National Park Service. https://irma.nps.gov/DataStore/Reference/Profile/2238788.

U.S. Geological Survey. 2018. *USGS EROD Archive - Aerial Photography*. https://www.usgs.gov/centers/eros/science/usgs-eros-archive-aerial-photography-aerial-photo-single-frames.

van Everdingen, R. O. 1998. *Multi-Language Glossary of Permafrost and Related Ground-Ice Terms in Chinese, English, French, German, Icelandic, Italian, Norwegian, Polish, Romanian, Russian, Spanish, and Swedish*. Boulder, CO: International Permafrost Association, Terminology Working Group, National Snow and Ice Data Center. http://nsidc.org/fgdc/glossary/.

The Department of the Interior protects and manages the nation's natural resources and cultural heritage; provides scientific and other information about those resources; and honors its special responsibilities to American Indians, Alaska Natives, and affiliated Island Communities.

NPS 953/180404, May 2022



Natural Resource Stewardship and Science
1201 Oakridge Drive, Suite 150
Fort Collins, CO 80525